國立臺灣大學理學院物理學研究所

碩士論文

Department of Physics

College of Science

National Taiwan University

Master Thesis

再探模糊暗物質中的核心-暈關係

Revisit the Core-Halo Relation in Fuzzy Dark Matter

廖品瑜

Pin-Yu Liao

指導教授: 薛熙于 博士

Advisor: Hsi-Yu Schive, Ph.D.

中華民國 112 年 8 月

August, 2023

doi:10.6342/NTU202303346

國立臺灣大學碩士學位論文

口試委員會審定書

再探模糊暗物質中的核心-暈關係

Revisit the Core-Halo Relation in Fuzzy Dark Matter

本論文係廖品瑜君（R10222063）在國立臺灣大學物理學研究所完成之碩士學位論文，於民國 112 年 7 月 26 日承下列考試委員審查通過及口試及格，特此證明

口試委員Oral examination committee:

許甫于	吳建宏	關志鴻
（指導教授Advisor		

系主任/所長Director: _____

doi:10.6342/NTU202303346

doi:10.6342/NTU202303346

致謝

衷心感謝薛熙于老師在過去兩年中的悉心指導，不吝傳授您的知識與技巧，讓我在這段時間裡學習到了眾多珍貴的研究方法和思考方式，更教導我如何聚焦研究的核心。同時，我也要感謝闕志鴻老師，您提供了眾多有益的見解，讓我能把物理想的更深入。此外，我要感謝吳建宏老師在口試時所提供的建議，完善了整篇論文。感謝實驗室的學長姐，讓我問了許多問題。特別感謝實驗室的蘇冠銘學長，即使是細節的問題也願意幫我解答，不懂的也會一起討論，更幫助我找出不少錯誤。同樣地，我要感謝我的家人，在過去兩年中給予了我無限的支持和鼓勵，偶爾還特地前來台北陪伴我。最後，我要感謝我的男朋友陳允中一直在我身旁，也給了我許多實用的建議。再次表達我最深的謝意！

doi:10.6342/NTU202303346

doi:10.6342/NTU202303346

摘要

在模糊暗物質（Fuzzy Dark Matter, FDM）中，暗物質暈的中心會形成孤子核心。先前的研究根據薛丁格-泊松方程和不確定性原理的縮放對稱性，預測核心質量與暈質量之間存在一個特定比例關係。然而模擬結果顯示大質量暈的結果與此比例關係偏離，卻缺乏合理的解釋。在本研究中，我們首先提出這種不一致部分是由於模擬分辨率不足，無法解析模糊暗物質的量子壓力，導致暈和核心都出現非物理壓縮所致。通過適當的分辨率，我們模擬中的 FDM 暈可以與冷暗物質（Cold Dark Matter, CDM）對應非常吻合，並且核心質量更接近預期值。在我們的後續分析中，我們通過將傳統的頂帽模型（Top-Hat Model）改善為廣泛接受的 NFW（Navarro-Frenk-White）剖面，提高了位能之準確性。此外，我們逐步分析了暈內部結構的溫度，發現在大質量之暈中，理論核心-暈關係中假設的等溫性並不滿足，導致核心質量被低估。我們還觀察到核心與周遭的溫度並不完全相同，而是存在一個常數差異，這種差異可能是由於孤子本身的特性所引起的。這些新發現修正了核心-暈關係並進一步讓我們對早期宇宙中凝聚核心如何形成有更深刻的理解。

關鍵字：模糊暗物質、數值模擬、暗物質暈、孤子核心、解析度

doi:10.6342/NTU202303346

doi:10.6342/NTU202303346

Abstract

In fuzzy dark matter (FDM), soliton cores form at the center of virialized halos. Previous studies predict a scaling relation between the core mass and halo mass due to the scaling symmetry of the Schrödinger-Poisson equation and the uncertainty principle. However, the simulation results deviate from this scaling relation for massive halos without an explanation. In this work, we first show that this inconsistency is partly due to insufficient simulation resolution for resolving the FDM quantum pressure, leading to unphysical compression of both halo and soliton. With adequate resolution, the FDM halo in our simulations can coincide very well with a CDM counterpart, and the soliton mass becomes closer to the expected value. In our subsequent analysis, we enhance the accuracy of the gravitational potential by substituting the top-hat model with the widely accepted NFW (Navarro-Frenk-White) profile. Furthermore, by analyzing the inner part of the halos, we find that the isothermal assumption is not valid for massive halos, resulting in an underprediction of soliton mass. Additionally, it has been observed that there exists a constant temperature differential between the core and its surrounding halo. This phenomenon may be attributed to the inherent characteristics of the soliton. These new findings pave the way for revising the core-halo relation and improving our understanding of soliton formation in the early universe.

Keywords: fuzzy dark matter, numerical simulation, dark matter halo, soliton core, resolution

doi:10.6342/NTU202303346

doi:10.6342/NTU202303346

Contents

doi:10.6342/NTU202303346

doi:10.6342/NTU202303346

List of Figures

doi:10.6342/NTU202303346

doi:10.6342/NTU202303346

List of Tables

doi:10.6342/NTU202303346

doi:10.6342/NTU202303346

Chapter 1 Introduction

1.1 Background and Motivation

The nature and properties of dark matter continue to be the subject of intense scientific scrutiny. While Cold Dark Matter (CDM) has been successful in explaining the large-scale structures of the universe, recent observations and theoretical developments have motivated alternative dark matter models that challenge the traditional assumptions [1–4]. One such intriguing model is fuzzy dark matter (FDM), which introduces a new perspective by postulating that dark matter particles possess an ultralight mass and exhibit wave-like behavior on galactic scales.

In the FDM framework, dark matter particles with masses on the order of 10^{-22} electron volts (eVs) form coherent wave-like structures, known as solitons, within galactic halos [5, 6]. These solitonic cores arise from the wave nature of FDM particles, and their existence can have profound implications for various astrophysical phenomena. Understanding the core-halo relation in FDM halos is of utmost importance as it is not only provides insight into the nature of FDM but also holds the potential to reconcile some of the persistent challenges faced by the CDM model.

The core-halo relation refers to the connection between the central density profiles of FDM halos and their overall mass distributions. Investigating this relation requires a detailed analysis of FDM simulations and a comprehensive understanding of the physical processes that shape the formation and evolution of solitonic cores. By studying the core-halo relation, we aim to reveal the fundamental properties of FDM and its impact on the structure of galaxies.

doi:10.6342/NTU202303346

This thesis builds upon the core-halo relation proposed by Schive et al. in 2014 [7]. However, the core mass deviate from the expected scaling relation for massive halos, and the underlying cause of this deviation remains unexplained [8, 9]. To address this discrepancy, we conducted simulations using the GAMER framework (Schive et al., 2018) [10]. GAMER is an adaptive mesh refinement tool that offers the advantage of automatic resolution adjustment, thereby optimizing resource utilization. By constructing two halos of different sizes through these simulations, we aim to shed light on the factors contributing to the observed deviations and provide insights into the underlying mechanisms at play.

By unraveling the intricacies of the core-halo relation in FDM, this research aims to contribute to our understanding of the nature of dark matter and provide valuable insights into the viability of FDM as a candidate for explaining the observed astrophysical phenomena. Ultimately, this investigation seeks to advance our knowledge of fundamental physics, cosmology, and the nature of the universe itself.

1.2 Outline of the Thesis

This thesis includes two halo simulations using a particle mass $m_\Phi = 2 \times 10^{-23}$ eV, with one exhibiting a mass of approximately $10^{12}\ M_\odot$ (referred to as the "heavy halo") and the other with a mass of around $9 \times 10^{10}\ M_\odot$ (referred to as the "light halo") (See Table 1.1). And the particle mass m_ψ is 2×10^{-23} eV. The objective of this thesis is to present a comprehensive analysis of the factors that contribute to the underestimation of soliton mass in FDM halos.

Table 1.1: Simulation halo properties at z = 0.

halo	mass ($M_\odot$)	radius (kpc)	concentration parameter
heavy	1.2e12	282	13.9
light	9.4e10	120	2.66

In the beginning, we discuss the soliton and halo properties and the core-halo relation in Sec. 2.1. Then we start exploring the cause of the core-halo relation deviation. The primary focus is on investigating the influence of resolution in FDM simulations and its

doi:10.6342/NTU202303346

crucial role in accurately capturing the properties of the halos (Sec. 2.3). Furthermore, a comparative analysis is conducted with Cold Dark Matter (CDM) simulations implemented using the GADGET2 code to ensure that the chosen resolution is adequate.

Another primary focus is to analyze the energy density directly. We improve the gravitational potential model from Top-Hat to NFW model and measure the kinetic energy directly in Sec. 3.1. We also investigate the temperature gradient in Sec. 3.2 and the soliton-halo equilibrium in Sec. 3.3. Other factors are also discussed in Sec. 3.4. The new prediction model is presented in Sec. 3.5.

Finally, we summarize our findings and discuss the implications of our results in Chap. 4.

doi:10.6342/NTU202303346

doi:10.6342/NTU202303346

Chapter 2 Resolving the Influence of Resolution

Simulation researchers often face the challenge of striking the right balance when it comes to resolution. Insufficient resolution can lead to the loss of crucial details, while overly high resolution can demand excessive computational resources. In this chapter, we will start by introducing the FDM core structure and the original core-halo relation. However, it has become evident that there is a noticeable deviation in the core-halo relation. Our investigations have revealed that the resolution in most FDM simulations is inadequate to resolve the quantum pressure. Consequently, the halo becomes overly concentrated, resulting in heavier solutions. To ensure adequate resolution, we conducted a thorough comparison with CDM simulations utilizing the GADGET2 code. Additionally, we found that it fits the NFW profile effectively. This comparative analysis emphasizes the importance of maintaining sufficient resolution throughout the entire volume of the halo.

2.1 Core Structure in Fuzzy Dark Matter

The FDM is described by Schrödinger-Poisson (SP) equation [11, 12]. The equation of expand universe is

$$\begin{aligned} \left[i\frac{\partial}{\partial \tau} + \frac{\nabla^2}{2} - aV \right] \psi = 0, \\ \nabla^2 V = 4\pi(|\psi|^2 - 1), \end{aligned} \tag{2.1}$$

doi:10.6342/NTU202303346

where

$$
\begin{aligned}
dx &= \left(\frac{3}{8\pi}H_0^2\Omega_{m0}\right)^{\frac{1}{4}}\left(\frac{m_\psi}{\hbar}\right)^{\frac{1}{2}}a^{-1}dx_{original},\\
d\tau &= \left(\frac{3}{8\pi}H_0^2\Omega_{m0}\right)^{\frac{1}{2}}a^{-2}dt,\\
\psi &= \left(\frac{m_\psi}{\rho_{m_0}}\right)^{\frac{1}{2}}\psi_{original},
\end{aligned}
\tag{2.2}
$$

where x is comoving length, τ is time, a is scale factor, V is gravitational potential, ψ is wave function, and H_0, Ω_{m0}, ρ_{m0} are the present Hubble parameter, matter density parameter and background mass density. We can import its scaling symmetry [11, 13] when $|\psi|^2 \gg 1$ and $a =$ const.. The SP equation remains unchanged under the transformation.

$$
(\tau, x, \psi, V) \rightarrow (\lambda^{-2}\tau, \lambda^{-1}x, \lambda^2\psi, \lambda^2 V). \tag{2.3}
$$

This equation has the capability to sustain stable and localized field configurations and form a solitonic core in the center of halo like Fig. 2.1 shows. Those solitons physical quantities can scale as below equation, where x_s, ρ_s, M_s, and E_s are the soliton radius, density, mass, and energy.

$$
(x_s, \rho_s, M_s, E_s) \rightarrow (\lambda^{-1}x_s, \lambda^4\rho_s, \lambda M_s, \lambda^3 E_s). \tag{2.4}
$$

The soliton density profile can be well fit by [14].

$$
\rho_c(x) = \frac{1.9a^{-1}(m_\Psi/10^{-23}\text{eV})^{-2}(x_c/\text{kpc})^{-4}}{[1+9.1\times10^{-2}(x/x_c)^2]^8}(M_\odot\text{pc}^{-3}). \tag{2.5}
$$

Here we introduce the notation x_c to represent the radius at which the density of the halo declines to one-half of its maximum value. Additionally, we define M_c as the enclosed mass within x_c. The subscript c denotes the core region of the halo. Our definition of core mass, $M(r \leq r_c)$, makes up about 25% of the total soliton mass. These definitions establish a quantitative basis for analyzing the core region's size and mass, enabling a systematic investigation of the core-halo relation.

doi:10.6342/NTU202303346

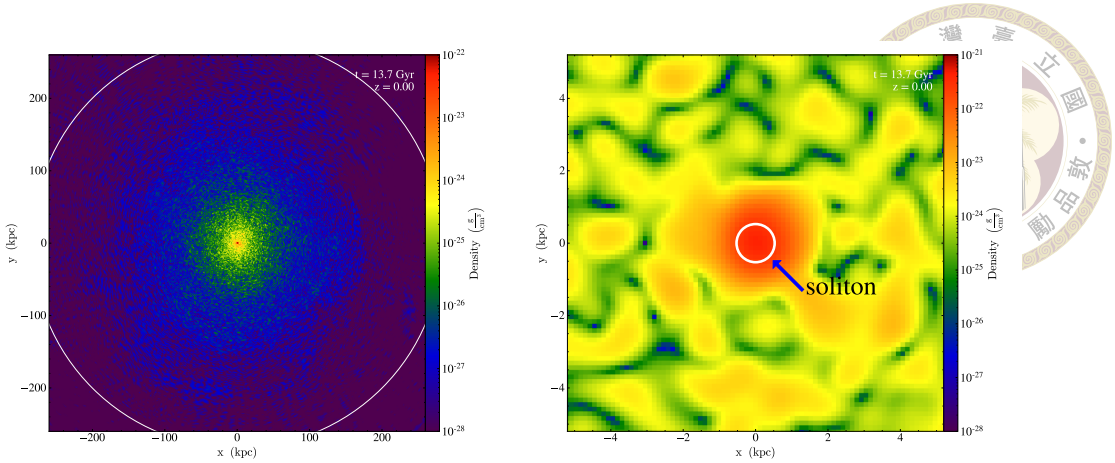

Figure 2.1: FDM halo and soliton core.

2.2 Traditional Core-Halo Relation

In our analysis, we make the assumption of isothermal equilibrium throughout the entire halo. This assumption implies that the energy density remains constant, irrespective of whether we are considering the halo or the core.

The halo virial mass M_h and its virial radius x_h are defined as

$$\begin{aligned} M_h &\equiv \left(\frac{4\pi x_h^3}{3}\right)\zeta(z)\rho_{m0}, \\ \zeta(z) &\equiv \frac{18\pi^2 + 82(\Omega_m(z)-1) - 39(\Omega_m(z)-1)^2}{\Omega_m(z)} \\ &\sim 350(180) \text{ at } z = 0(z \geq 1). \end{aligned} \tag{2.6}$$

The virial mass definition [15] remains consistent for both CDM and when an object surpasses the Jeans mass during its collapse. This is due to the similarity in dynamics between the two scenarios, where the Eikonal approximation of wave dynamics to particle dynamics holds true until virialization occurs.

From Eq. 2.1 and assuming $a = const.$ and also zero background density, one expects that the final relaxed state should lose the memory of its initial configuration and thus depends only on the globally conserved quantities, namely, the total mass M and energy E (assuming there is no net angular momentum). We suppose that the energy density, i.e.

doi:10.6342/NTU202303346

temperature, between soliton and halo, might be in equilibrium. In our study, we employ the notation "s" to represent soliton, "c" to denote the core.

$$\begin{aligned} \frac{|E'_s|}{M'_s} &= \frac{|E'_h|}{M'_h}, \\ M' &= \int |\psi|^2 d^3x', \\ E'_k = \frac{1}{2}\int |\nabla'\psi'|^2 d^3x',\ E'_p &= \frac{1}{2}\int |\psi'|^2 V' d^3x'. \end{aligned} \tag{2.7}$$

Here the apostrophe means red shift independent and use the unit according to Eq. 2.2. According to the soliton scaling, $E_s X_s^3$ and $M_s x_s$ are two constants. The equation will become

$$\frac{|E'_s|}{M'_s} = \frac{(|E'_s|x'^3_s)M'^2_s}{(M'_s x'_s)^3} = \left(\frac{M'_s}{4.3}\right)^2 \sim M'^2_c. \tag{2.8}$$

Based on the previous study [7], we estimated the gravitational potential utilizing the spherical collapse model, specifically the Top-Hat model. The Top-Hat model provides a framework for analyzing the energy associated with this gravitational potential. By employing the virial theorem, we can determine the total energy of the system. The energy associated with the Top-Hat model can be expressed as Eq. 2.9:

$$\begin{aligned} |E_h| &= |E_k + E_p| = |\tfrac{1}{2}E_p|. \\ \Rightarrow E_p &= -4\pi\left(\frac{M}{\frac{4}{3}\pi r^3}\right)^2 \frac{4}{3}\pi \int_0^R r^4 dr = -\frac{3M^2}{5R}. \end{aligned} \tag{2.9}$$

Combine Eq. 2.7, Eq. 2.8 and Eq. 2.9, the equation becomes:

$$M'_c = \sqrt{\frac{\frac{3M'^2_h}{10x'_h}}{M'_h}} = \sqrt{\frac{3M'_h}{10x'_h}}. \tag{2.10}$$

Since the soliton cannot be larger than halo, set $M_{min,0}$ to be the minimal M_h at $z = 0$.

doi:10.6342/NTU202303346

Note that $\frac{M_{min,0}}{4} = \frac{M_s}{4} \sim M_c$.

$$
\begin{aligned}
\frac{M_{min,0}}{4} &= M_{min,0}^{\frac{1}{3}} \left(\frac{27}{1000} \frac{4\pi\zeta(0)\rho_{m0}}{3} \right)^{\frac{1}{6}}, \\
M_{min,0} &= 8 \left(\frac{9}{250} \pi\zeta(0)\rho_{m0} \right)^{\frac{1}{4}}, \\
&= 375^{-\frac{1}{4}} 32\pi\zeta(0)^{\frac{1}{4}} \left(\frac{H_0 m_\psi}{\hbar} \right)^{-\frac{3}{2}} \Omega_{m0}^{-\frac{3}{4}} \rho_{m0}, \\
\Rightarrow M_c &= \frac{1}{4} a^{-\frac{1}{2}} \left(\frac{\zeta(z)}{\zeta(0)} \right)^{\frac{1}{6}} \left(\frac{M_h}{M_{min,0}} \right)^{\frac{1}{3}} M_{min,0}.
\end{aligned}
\tag{2.11}
$$

That is the core-halo relation in [7]. In the Fig 2.2, we compare the predicted and simulated masses. It is evident that the core masses from the simulation are higher than those predicted in the heavy halo region.

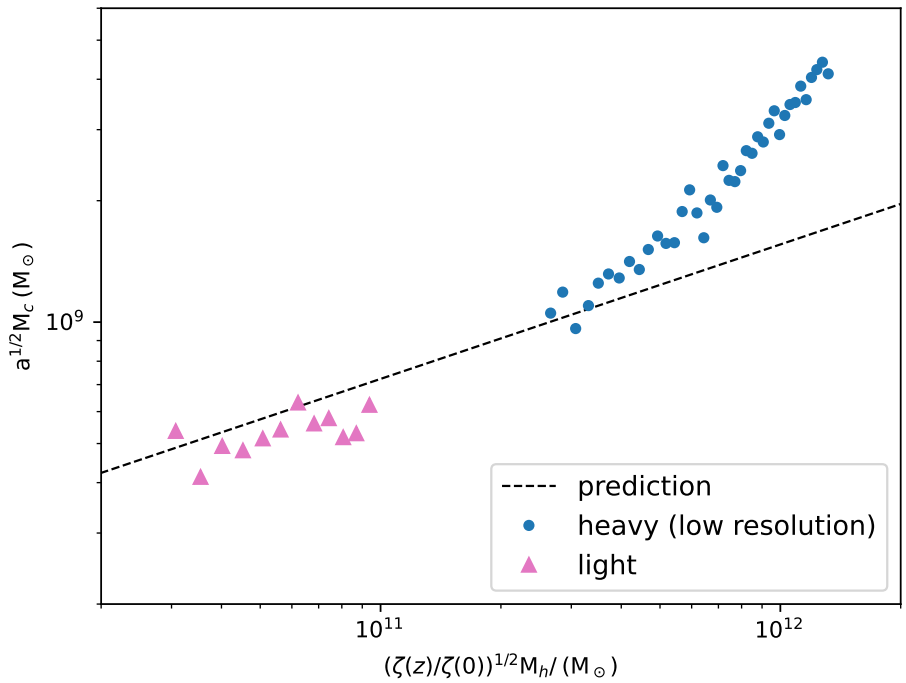

Figure 2.2: Core-halo relation. The simulation core masses are higher than predictios in the heavy halo.

doi:10.6342/NTU202303346

2.3 Ensuring Sufficient Resolution

2.3.1 Increasing Resolution

The density profile can be observed in Fig. 2.3. In the case of the low-resolution simulation, the halo appears to be excessively concentrated. One exploration of this observation is that the low resolution of the simulation does not accurately resolve the quantum pressure, which is essential for balancing gravitational forces. Consequently, the halo becomes overly concentrated and hotter, leading to an increase in the soliton mass. The density profile obtained from the high-resolution simulation, on the other hand, is less concentrated and has a lighter core mass. Note that the low-resolution simulation is actually the default resolution of GAMER, which is almost higher than other simulation tools. It appears that in most of the previous research, the resolution has been insufficient to fully address this issue. The resolution region is shown in Fig. 2.4.

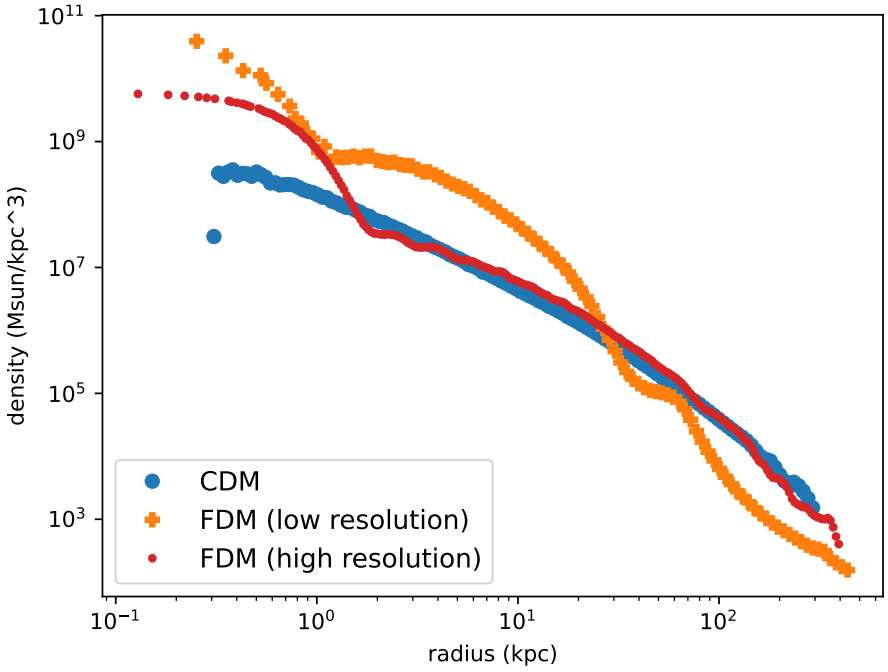

Figure 2.3: The density profile comparison. The low resolution is the default resolution of GAMER. The high resolution one and CDM simulation are consistent at the halo region.

doi:10.6342/NTU202303346

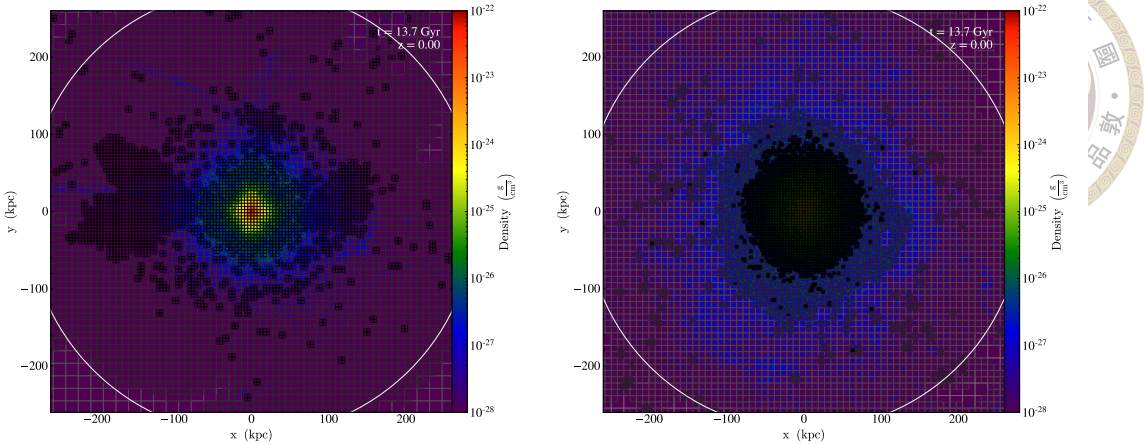

Figure 2.4: A comparison of halo slice densities with different grid resolutions. The left panel shows the highest resolution at 0.25 kpc. The right panel with the center resolution increased to 0.125 kpc. The circle is its halo region.

2.3.2 Comparing FDM and CDM Simulations

To obtain the right balance between accuracy and computational efficiency, it is important to choose an optimal resolution for simulations. We can use a widely-used simulation of CDM as a starting point since it behaves similarly to FDM on large scales.

We conducted simulations using the GADGET2 code with identical initial conditions to compare the density profiles of the halo. It shows a close agreement between the density profiles obtained from the FDM and CDM simulations (blue dots in Fig. 2.3). The agreement between the two density profiles validates our analysis and allows for a robust examination of the core-halo relation in FDM.

For both halos, a comparison was conducted to assess the consistency between CDM and FDM simulations. In Fig. 2.5, we examined the density profiles and compared them with the corresponding CDM profile. The density closely resembles the FDM profile throughout, except in the region corresponding to the soliton. Furthermore, we carried out a comparison of the obtained results with the widely accepted NFW (Navarro-Frenk-White) profile [16]. The comparison revealed a good fit of the density profile, indicating that the simulations align well with the NFW profile.

doi:10.6342/NTU202303346

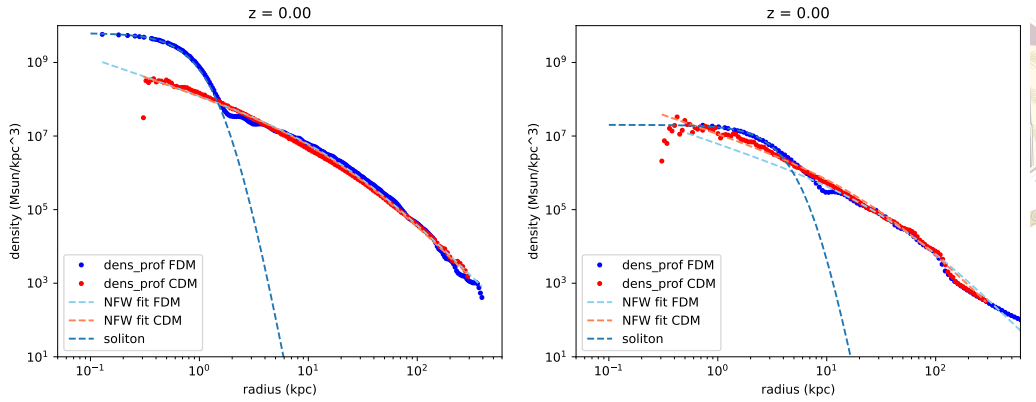

Figure 2.5: Density profile compare to CDM and NFW profile. Left one is heavy halo, and the right one is light halo. Both are consistent with CDM and NFW profiles, which indicates that the resolution is sufficient.

2.3.3 Core-Halo Relation with Sufficient Resolution

The core-halo relation with higher resolution is shown in Fig. 2.6. The core mass is lower than the low resolution case.

doi:10.6342/NTU202303346

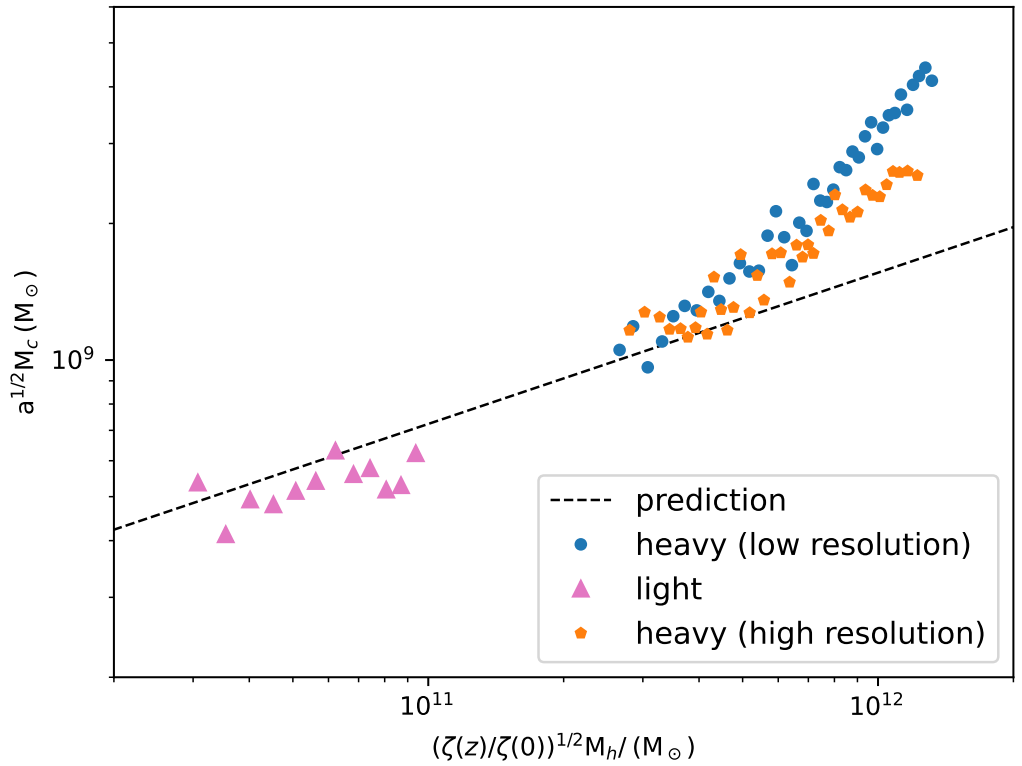

Figure 2.6: Core-halo relation. The simulation core mass decreases when resolution is sufficient.

In summary, our investigation highlighted the importance of resolution in accurately capturing the density profile of dark matter halos. In most of the previous studies, the resolution is not high enough. By increasing the resolution, we were able to obtain a density profile that more closely resembled the CDM simulation and expected NFW profile. Furthermore, the improved resolution resulted in a reduction of the core mass, which brought the core mass closer to the core-halo relation prediction. This finding indicates that the resolution plays a crucial role in determining the core mass. In the next chapter, we will investigate the core-halo relation in greater detail by conducting a comparative analysis of the two halos.

doi:10.6342/NTU202303346

doi:10.6342/NTU202303346

Chapter 3 Investigating Equilibrium of Energy

This chapter focuses on revising the core-halo relation based on enough resolution result from the previous chapters. First, we will revise the potential energy model into NFW, which makes the potential energy higher to make the prediction mass larger. Then we discuss the limitations of the isothermal assumption, particularly for massive halos, and how it under-predicts the soliton mass. Last we'll introduce the soliton-halo energy equilibrium. The subsequent sections of this chapter are dedicated to a comprehensive analysis of the various factors contributing to the underprediction phenomenon. Each factor is examined individually to understand its influence on the core-halo relation and its role in causing whether over or underestimation.

3.1 NFW Potential Energy Model

In Sec. 2.2, we computed the gravitational potential using the Top-Hat model within the framework of the spherical collapse model. However, in Fig. 2.5 we can see that the density is not a constant, is more like a NFW profile. It is imperative to transition from the Top-Hat model to the NFW profile [17–19]. This transition necessitates considering the concentration parameter, denoted as c, as the energy of the halo becomes a function of this parameter. By adopting the NFW profile, we can incorporate the influence of the concentration parameter on the gravitational potential, aligning our analysis with the

doi:10.6342/NTU202303346

insights presented in the aforementioned papers.

$$
\begin{aligned}
E_p &= \frac{1}{2}\int_0^{R_h} \Phi(r) dM_{\text{shell}}(r), \\
&= \frac{1}{2}\int_0^{R_h} \left[-\frac{4\pi G\rho_0 R_s^3}{r} ln\left(1+\frac{r}{R_s}\right) + \frac{4\pi G\rho_0 R_s^3}{R_h}\frac{c}{1+c} \right] \frac{4\pi r^2 \rho_0}{\frac{r}{R_s}\left(1+\frac{r}{R_s}\right)^2} dr, \\
&= \frac{GM^2}{2R_h}\frac{2c(1+c)ln(1+c) - 2c^2 - c^3}{\left[(1+c)ln(1+c) - c\right]^2}.
\end{aligned}
\tag{3.1}
$$

Within the range of halo concentration parameters (4-40), the potential energy exceeds that of the Top Hat model by approximately 60% to 270%. This significant increase in potential energy results in a substantial rise in the predicted mass of solitons.

We import the concentration parameter depends on halo mass and redshift [20]. They assumed for a given halo mass, the concentrations follow a lognormal distribution with a standard deviation of approximately $\rho_{logc} \simeq 0.12$.

$$
c(M,z) = \frac{4.67}{1+z}\left(\frac{M(z)}{10^{14}h^{-1}M_\odot}\right)^{-0.11}. \tag{3.2}
$$

doi:10.6342/NTU202303346

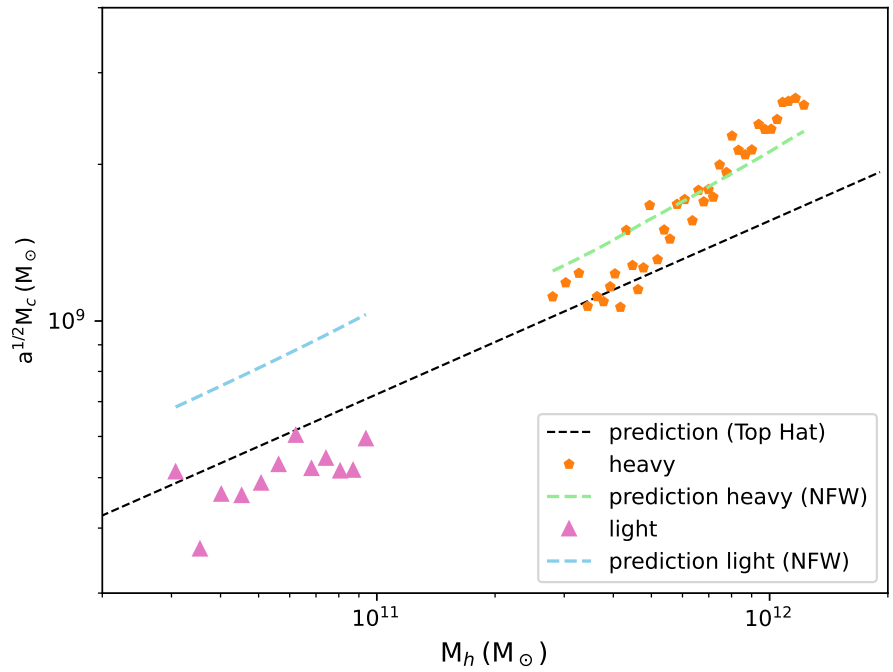

Figure 3.1: Core-Halo relation with NFW potential. The black dash line is old core-halo relation by Top-Hat. Revising the potential model into NFW makes the prediction higher.

After revise the NFW potential, we can get the new core-halo relation (Fig. 3.1). The dash line is old core-halo relation by [7]. The new core-halo relation is much closer to the simulation result in heavy halo. However, in small halo the prediction is higher a lot.

3.2 Temperature Gradient

In Section 2.2, we studied the core-halo relation and its link to energy equilibrium in the system. We can use the virial theorem to convert potential energy into kinetic energy. To validate the assumption of isothermality, we looked into the velocity dispersion σ of the system. The analysis with the Jeans equations revealed a radial dependence of velocity dispersion within the halo. The kinetic energy $E_k(r)$ at a given radius r in the halo is given by $E_k(r) = \frac{1}{2} m_r \sigma_r^2$, where m_r is the mass within that radius, and σ_r is the corresponding velocity dispersion.

The velocity for the FDM system is described by Eq. 3.3. It includes two components: P_{QP}, which accounts for the quantum pressure caused by the density gradient, and

doi:10.6342/NTU202303346

P_{Bulk}, which accounts for the bulk motion induced by the wave function phase gradient. The velocity dispersion σ is calculated as the square root of the difference between the average squared velocity $\langle v^2 \rangle$ and the squared average velocity $\langle v \rangle^2$. In the halo region, The average velocity $\langle v \rangle$ is close to zero, while in the soliton region, it is non-zero. The analytical soliton solution only contains the quantum pressure velocity directed toward the center. To fully account for the soliton's kinetic energy, we also need to consider the non-zero average velocity $\langle v \rangle$ in the soliton part.

$$
\begin{aligned}
E_k &= \rho[v_{QP}^2 + v_{Bulk}^2], \\
v_{QP} &= \frac{\hbar}{\rho}[\phi_{Real}(\vec{r})\nabla\phi_{Real}(\vec{r}) + \phi_{Imag}(\vec{r})\nabla\phi_{Imag}(\vec{r})], \\
v_{Bulk} &= \frac{\hbar}{\rho}[\phi_{Real}(\vec{r})\nabla\phi_{Imag}(\vec{r}) + \phi_{Imag}(\vec{r})\nabla\phi_{Real}(\vec{r})], \\
\rho &= m_{22}|\phi(\vec{r})|^2.
\end{aligned}
\tag{3.3}
$$

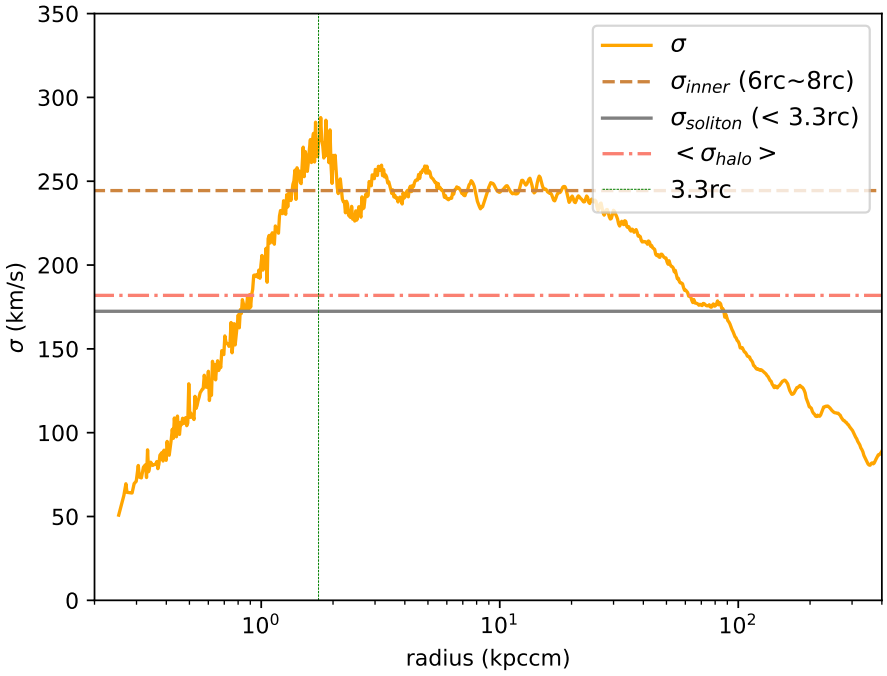

Figure 3.2: The velocity dispersion of heavy halo.

doi:10.6342/NTU202303346

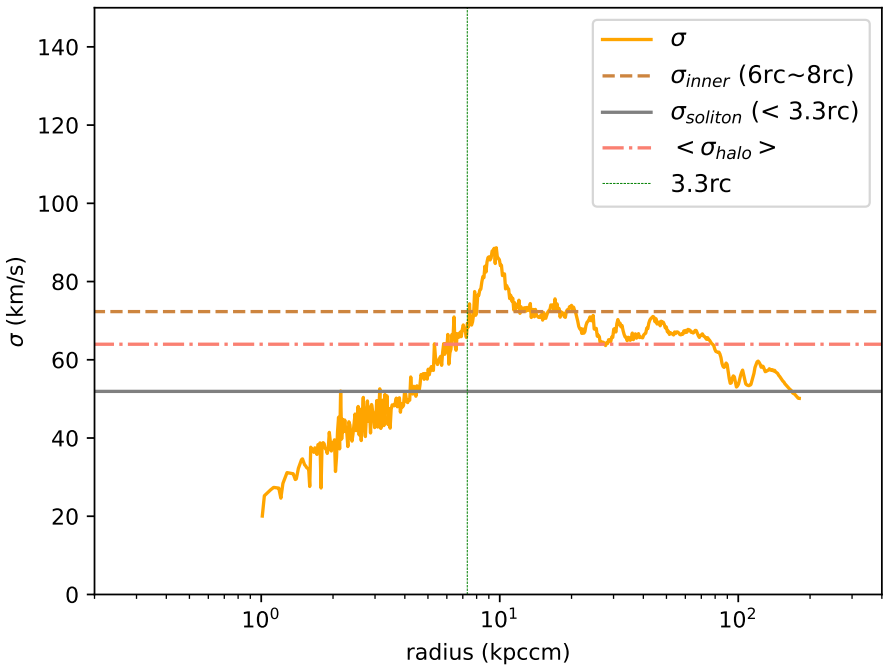

Figure 3.3: The velocity dispersion of light halo.

Our main objective was to examine the distribution of σ across the halo to see if it aligns with the isothermal model assumptions. Expanding on previous studies, where the soliton's average $\sigma_{soliton}$ and the halo's σ_{halo} were assumed to be in equilibrium, we now aim to investigate the dynamics in different regions. The σ function of radius is shown at Fig. 3.2 and Fig. 3.3.

In our investigation, we examined the velocities of the inner part (6 to 8 r_c) of the halo and compared them with the velocities of the entire halo. Surprisingly, we discovered that the ratio of σ between the inner part and the whole halo was not consistent. Figure3.4 illustrates that the σ ratio is higher than 1, indicating that the inner part of the halo is hotter compared to the rest of the halo. Notably, when analyzing heavy halos, we observed an increasing trend in the σ ratio. This temperature gradient implies that heavy halos show a departure from a constant value, indicating substantial differences in the dynamics within their inner regions compared to the entire halo. On the other hand, light halos exhibited a relatively constant σ ratio. This variation in the σ ratio provides valuable insights into the intricate dynamics and structure of different halo types, warranting further exploration and analysis to uncover the underlying mechanisms driving these observations.

doi:10.6342/NTU202303346

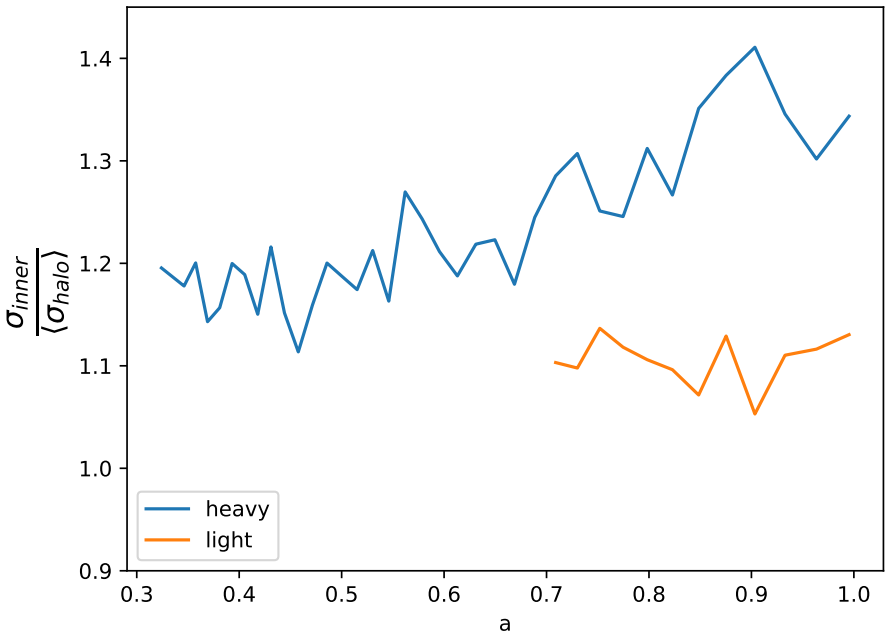

Figure 3.4: Temperature gradient comparison. The ratio larger than one reveals non-isothermal properties within the halos, with hotter temperatures at their centers. In heavy halos, there is an observable trend of the temperature gradient increased.

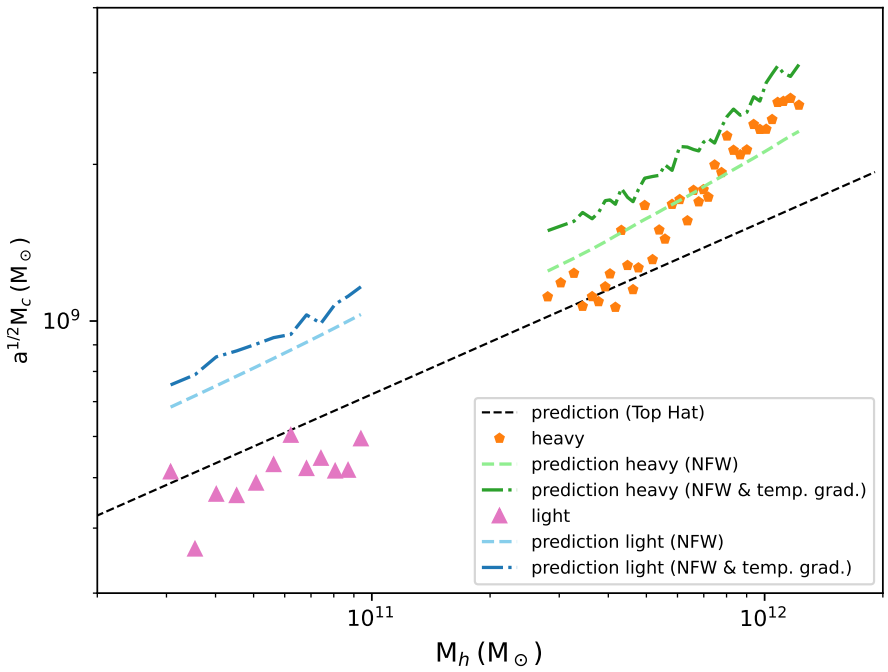

Figure 3.5: Core-Halo relation with temperature gradient. The temperature gradient's upward trend results in a prediction with a slope that better corresponds to the simulation data, albeit at a higher magnitude.

doi:10.6342/NTU202303346

Bring this result back to the core-halo relation, see Fig 3.5. the increasing temperature gradient leads to a prediction with a slope that aligns better with the simulation data, albeit at a higher level. And it also makes the prediction of light halo much higher than the simulation result. Because of this overestimation, we need to further consider the soliton-halo equilibrium.

3.3 Soliton-Halo Equilibrium

We make the assumption that the soliton is located near the inner region of the halo, implying a similarity in their respective energy levels. We specify the soliton range as the region within 3.3 times the r_c from the halo center, encompassing 95% of the soliton's energy.

Comparing the σ values of solitons and inner halos yields a noteworthy ratio (see Fig. 3.6). Remarkably, in heavy halo, this ratio closely approximates the square root of 0.5, equating to approximately 0.75. Even in the case of light halos, this trend persists as time progresses. This behavior highlights a fundamental aspect of the system's dynamics and underscores the significance of this σ ratio as a key characteristic in both heavy and light halos over time. However, to ensure the accuracy and reliability of our observations, further theoretical calculations are needed. Additionally, expanding our analysis to encompass a broader range of halo configurations and characteristics would enhance the robustness of our findings.

doi:10.6342/NTU202303346

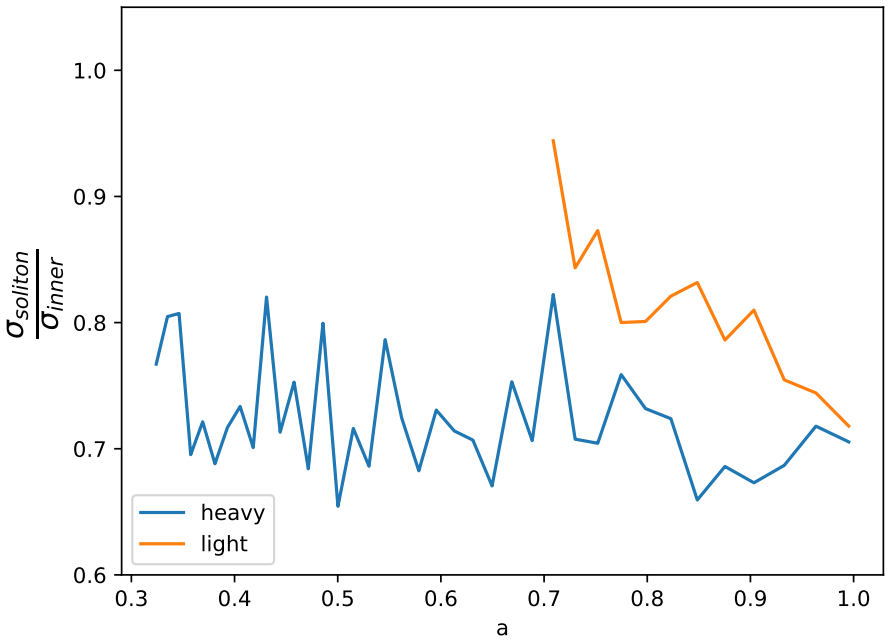

Figure 3.6: The σ ratio of the core part and inner part. It's close to the square root of 0.5 in heavy halo.

We also include this equilibrium in the core-halo relation. The Fig. 3.7 is the core-halo relation with soliton-halo equilibrium. It's closer to the simulation core mass. Though it still overestimates the light halo, it's much better than the previous result.

doi:10.6342/NTU202303346

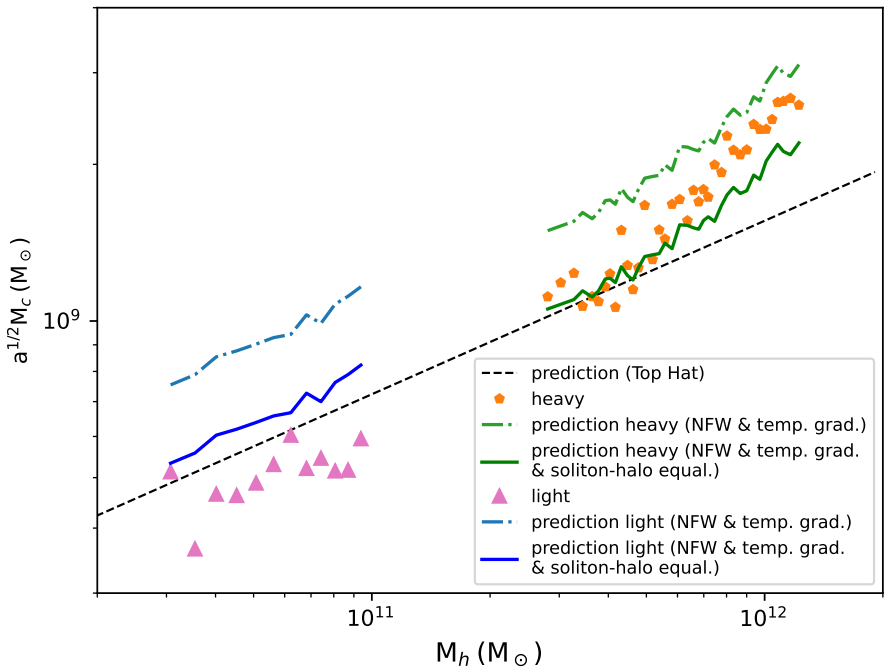

Figure 3.7: Core-Halo relation with soliton-halo equilibrium. This equilibrium reduces the predicted core mass to bring it into closer alignment with the core mass observed in the simulations.

3.4 Other Contributing Factors

Though we've already get a better core-halo relation, but there are still some deviation. Here we explore other factors that might contribute to the deviation.

3.4.1 Theoretical v.s. Fitted Concentration Parameter

In Sec.3.1, we use the theoretical concentration parameter by Eq. 3.2 to calculate the potential energy. However, the concentration parameter may not be exactly equal to the simulation. Here we fit the halo with the NFW profile to get the concentration parameter (like Fig. 2.5 shows). The heavy halo's concentration parameters are bigger than theoretical, while the light halo's are the opposite.

doi:10.6342/NTU202303346

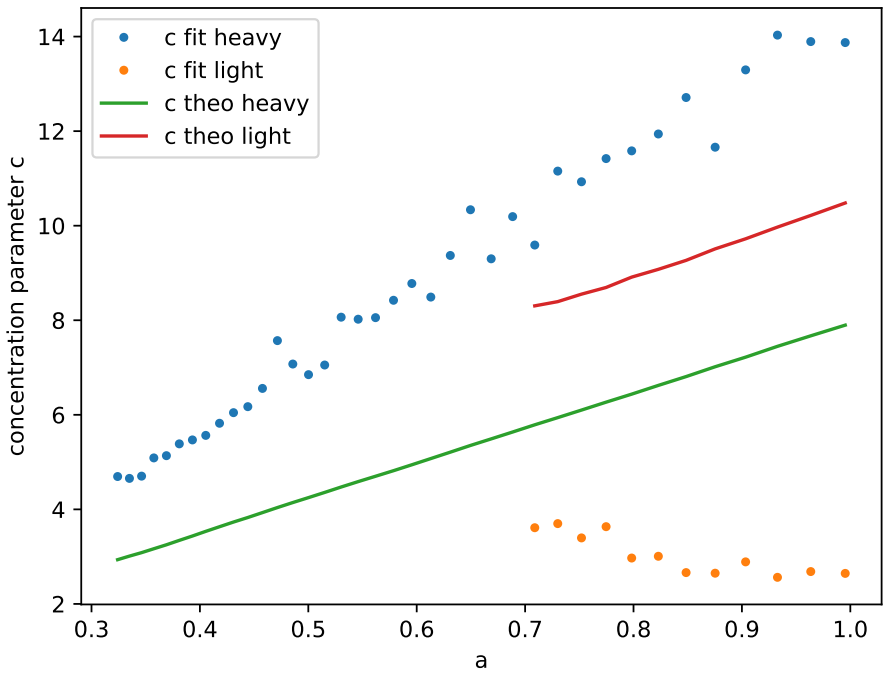

Figure 3.8: The concentration parameter c comparison. The concentration parameters of the heavy halo are larger than theoretical one, whereas for the light halo, the situation is reversed.

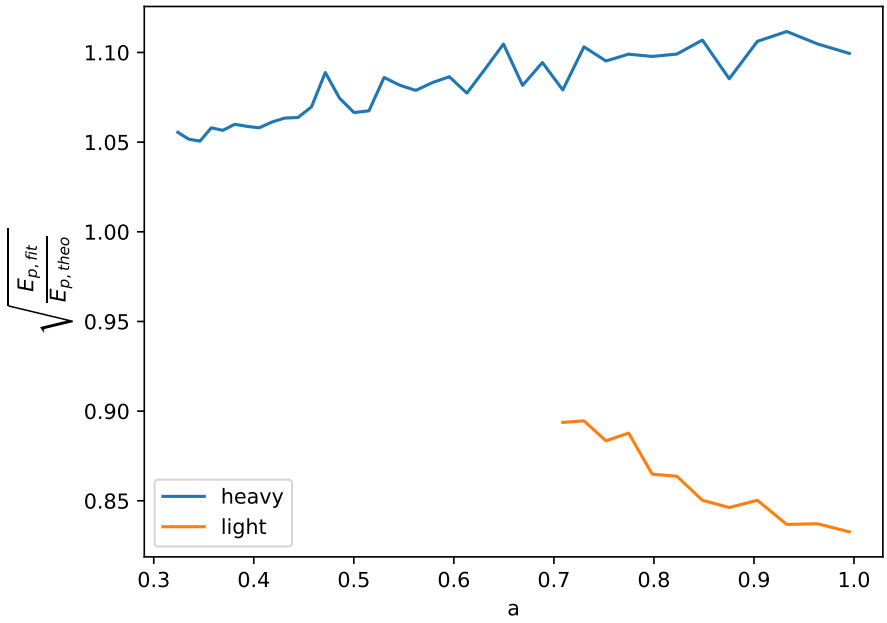

Figure 3.9: The ratio of $\sqrt{\frac{E_{p,fit}}{E_{p,theo}}}$. The ratio of heavy halos is greater than 1, which means that the forecast is underestimated. The light halo has the opposite situation.

doi:10.6342/NTU202303346

The Fig. 3.9 shows the ratio of $(\frac{E_{p,fit}}{E_{p,theo}})^{0.5}$. $E_{p,theo}$ uses the theoretical concentration parameter derived from Equation 3.2. While the theoretical concentration parameter exhibits scatter, it is considered acceptable and within the expected range. The ratio of $(\frac{E_{p,fit}}{E_{p,theo}})^{0.5}$ might explain why the prediction in Fig. 3.7 is lower than the simulation result in heavy halo while higher than simulation result in light halo.

It is important to note that the y-axis in the figures represents the square root of the energy ratio. This choice of representation is intended to facilitate a direct comparison with the soliton mass in subsequent analyses.

3.4.2 NFW fitting

It is also essential to assess the degree to which the halo aligns with the NFW profile. This evaluation involves examining whether the simulation data can be adequately described by the NFW model and determining the corresponding concentration parameter. Fig. 3.10 is the square root of potential energy and demonstrates the agreement between the simulation data and the NFW fitting. $E_{p,sim}$ is calculated by Eq. 3.4, and $E_{p,fit}$ is by fitting the halo with an NFW profile and determining the corresponding concentration parameter. The results are very close to 1, indicating that the NFW profile is a good fit for the simulation data.

$$
\begin{aligned}
E_p &= \frac{1}{2}\int_0^{R_h} \Phi(r) dm_r \\
\Phi(r) &= \int_0^{R_h} \begin{cases} \dfrac{G dm_{r'}}{r'}\dfrac{r'}{r} \ , \ r' < r \\ \dfrac{G dm_{r'}}{r'} \ , \ r' > r \end{cases}
\end{aligned}
\tag{3.4}
$$

doi:10.6342/NTU202303346

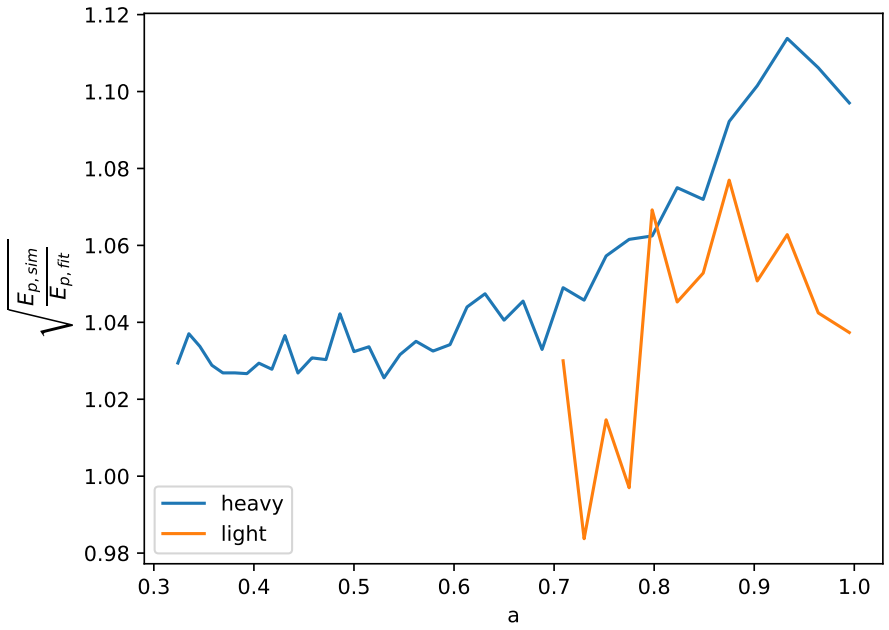

Figure 3.10: The ratio of $\sqrt{\frac{E_{p,sim}}{E_{p,fit}}}$. The results are very close to 1, indicating that the NFW profile is a good fit for the simulation data.

3.4.3 Virial Condition

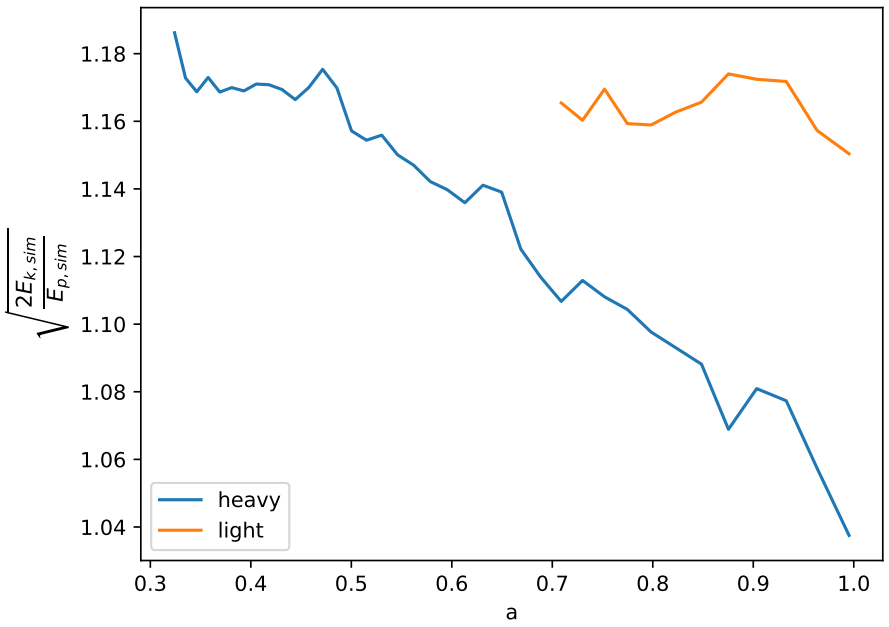

Figure 3.11: The ratio of $\sqrt{\frac{E_{p,sim}}{2E_k}}$. The ratio greater than 1 means the prediction is underestimated.

doi:10.6342/NTU202303346

Although we assume a virial condition, we proceed to verify its correctness by examining the potential energies determined from the simulations. In Fig. 3.11, it is observed that the quantity $(\frac{2E_k}{E_p})^{0.5}$ approaches a value close to 1 as time progresses in heavy halo. The virial condition is varies among different halos, implying that each halo possesses its own distinct value. Relaxed halos are defined to have values of this quantity less than 1.35 [21]. Based on this criterion, our halo can be classified as a relaxed halo.

3.4.4 Soliton Energy Ratio

Despite the analytical soliton model's assumption of having no bulk energy and consisting solely of quantum pressure, our analysis revealed the existence of non-negligible bulk energy contributions. As discussed in Schive et al. 2020 [22], solitons undergo a random walk process. This phenomenon implies that a portion of the soliton's energy is allocated to the bulk energy component, contrary to the initial assumption of pure quantum pressure dominance.

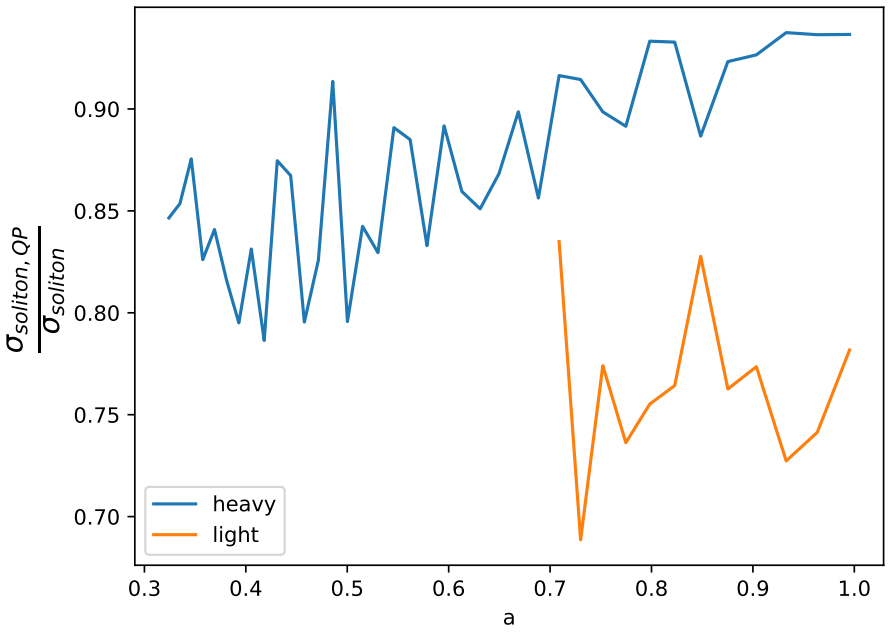

Figure 3.12: The QP energy ratio. Not all of the energy will contribute to forming a soliton, which results in predictions higher than the simulation data.

To quantify this energy distribution more accurately and facilitate a precise conver-

doi:10.6342/NTU202303346

sion from energy to mass, we calculated the ratio of the total energy to the energy derived from quantum pressure. The findings are depicted in Fig. 3.12, which showcases the temporal evolution of this ratio. Notably, when the soliton is less stable and light, it exhibits a higher energy content and a higher propensity for energy redistribution between the quantum pressure and bulk energy components.

3.5 Revisiting core-halo relation

We combined all the mentioned factors and tried to get a new prediction of soliton mass. To elucidate the process by which the halo mass (M_h) translates into the soliton mass (M_c), we have created a flow chart, as depicted in Fig. 3.13. This diagram provides a visual representation of the steps involved in the conversion. This will closed to the simulation core mass see Fig. 3.15. We list all the factors below and put them together, so we can easily see which factor might be not important. To enhance clarity, we have employed different text colors in the flow chart (Fig. 3.13) to convey specific information. Blue text signifies theoretical calculations or theoretical deviations from expected values, while red text indicates ratios or measurements obtained through actual simulation. The soliton perfectness is the ratio between measured soliton mass and predict soliton mass.

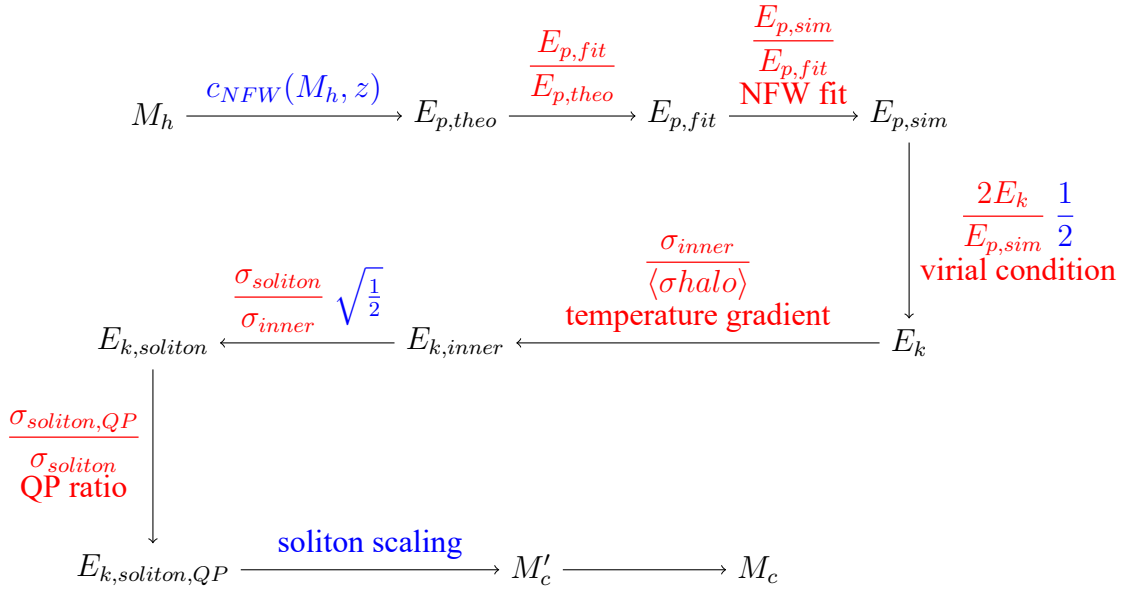

Figure 3.13: Flow chart: from halo mass to soliton mass.

doi:10.6342/NTU202303346

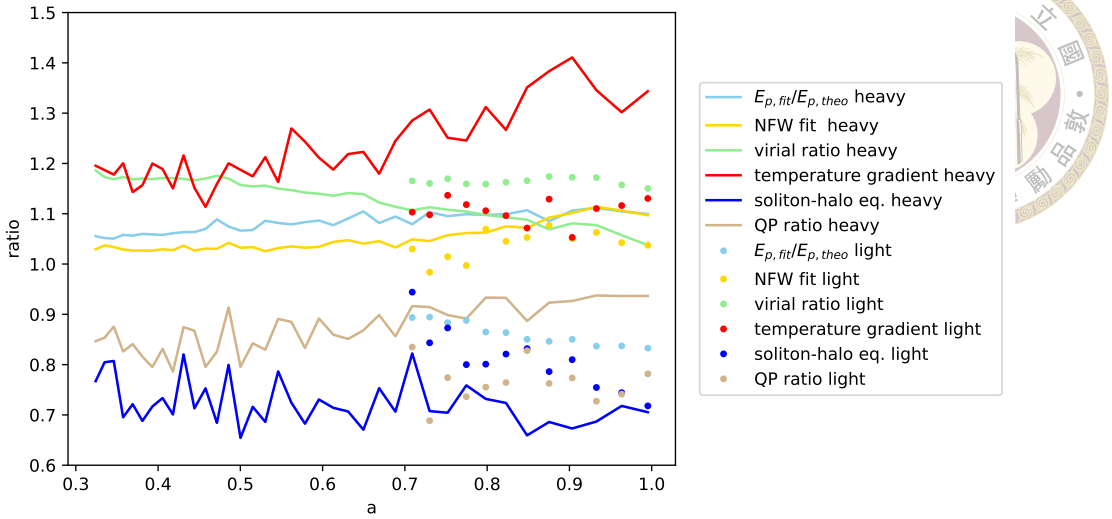

Figure 3.14: The factors that influence the core-halo relation. The core mass is directly affected by the magnitude of the ratio: a higher ratio leads to a larger predicted mass, while a lower ratio results in a smaller predicted mass.

In summary, we have conducted a comprehensive analysis to predict the soliton mass (M_c) based on the halo mass (M_h). We integrated various factors and observations to refine our predictions. Through this analysis, we have identified the significance of different factors. By considering these factors and observations collectively, we can adopt a more direct approach. This approach allows us to make predictions that closely align with simulation results, as demonstrated by the comparison of soliton core mass in Figure 3.15.

doi:10.6342/NTU202303346

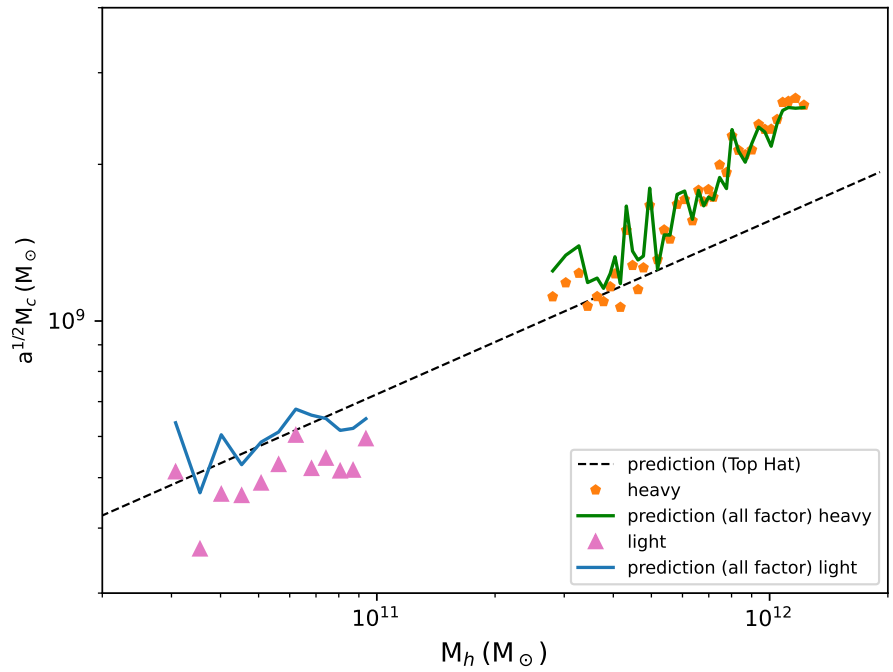

Figure 3.15: Core-halo relation with above factors. It's much closer to the simulation result.

The core-halo relation can be significantly improved by taking into account the NFW potential energy, temperature gradient, and soliton-halo equilibrium. This comprehensive approach ensures a more accurate representation of the system, aligning our predictions much more closely with simulation results. Furthermore, by combining and evaluating multiple factors, we have improved the accuracy and precision of our predictions for soliton mass based on halo mass, leading to a better understanding of the relationship between these two quantities.

doi:10.6342/NTU202303346

Chapter 4 Discussion and Conclusion

In Chap. 2, our investigation has provided valuable insights into the interplay between resolution and the accuracy of density profiles in dark matter halos. By increasing the resolution of our simulations, we reduce the halo temperature, which in turn leads to a further decrease in the core mass. To further validate our results and ensure the adequacy of our resolution, a valuable avenue for future research would be to compare our findings with those obtained from GADGET2 simulations based on CDM models. By comparing our density profiles with those generated by CDM simulations, we can assess the level of agreement and verify that our resolution is indeed adequate. This comparative analysis would provide further confidence in the reliability and accuracy of our density profiles and enhance the robustness of our conclusions.

Additionally, in Chap 3, we conducted an extensive analysis to predict the soliton mass (M_c) based on the halo mass (M_h). Through three main factors NFW potential energy, temperature gradient, and soliton-halo equilibrium, we can align our predictions much more closely with simulation results. Through the integration of other factors and observations, we refined our predictions and identified their significance. The flow chart provided a clear visual representation of the conversion process, highlighting the relevant steps involved. This refined prediction approach offers valuable insights into the relationship between soliton and halo masses.

In order to enhance our understanding of the core-halo relationship, it is imperative to explore various aspects associated with the temperature gradient observed predominantly in heavy halos. A potentially fruitful avenue of investigation involves an in-depth examination of the relationship between the temperature gradient and halo mass. Additionally,

doi:10.6342/NTU202303346

elucidating the isothermal connection between the inner part of the halo and the soliton could provide valuable insights. A pertinent question arises as to whether the soliton's degrees of freedom, being half that of fuzzy dark matter, contribute to this relationship. Moreover, it is plausible that the mass of the soliton may influence the QP (quantum pressure) ratio. Thoroughly investigating these factors would undoubtedly contribute significantly to our comprehension of the intricate interplay between core properties and halo characteristics.

Regarding other contributing factors, it is essential to conduct more halo simulations to confirm whether they have a minor impact on the overall core-halo relationship. A comprehensive investigation of these elements will lead to a more comprehensive and accurate understanding of the complex dynamics between core properties and halo behavior.

Overall, our findings contribute to the ongoing research on dark matter halos and solitons, enhancing our understanding of their formation, structure, and dynamics. The insights gained from this study open avenues for further investigation and deepen our comprehension of the fundamental properties of the universe.

doi:10.6342/NTU202303346

References

[1] G. Kauffmann, S. D. M. White, and B. Guiderdoni. The formation and evolution of galaxies within merging dark matter haloes. Mon Not Roy Astron Soc, 264(1):201–218, 09 1993.

[2] Anatoly Klypin, Andrey V. Kravtsov, Octavio Valenzuela, and Francisco Prada. Where are the missing galactic satellites? Astrophys J, 522(1):82–92, sep 1999.

[3] Ben Moore, Sebastiano Ghigna, Fabio Governato, George Lake, Thomas Quinn, Joachim Stadel, and Paolo Tozzi. Dark matter substructure within galactic halos. Astrophys J, 524(1):L19–L22, oct 1999.

[4] Jurg Diemand, Michael Kuhlen, and Piero Madau. Dark matter substructure and gamma-ray annihilation in the milky way halo. Astrophys J, 657(1):262–270, mar 2007.

[5] Wayne Hu, Rennan Barkana, and Andrei Gruzinov. Fuzzy cold dark matter: The wave properties of ultralight particles. Phys. Rev. Lett., 85:1158–1161, Aug 2000.

[6] P. J. E. Peebles. Fluid dark matter. Astrophys J, 534(2):L127–L129, may 2000.

[7] Hsi-Yu Schive, Ming-Hsuan Liao, Tak-Pong Woo, Shing-Kwong Wong, Tzihong Chiueh, Tom Broadhurst, and W-Y. Pauchy Hwang. Understanding the core-halo relation of quantum wave dark matter from 3d simulations. Phys Rev Lett, 113(26), Dec 2014.

[8] Philip Mocz, Mark Vogelsberger, Victor H. Robles, Jesú s Zavala, Michael Boylan-Kolchin, Anastasia Fialkov, and Lars Hernquist. Galaxy formation with BECDM

doi:10.6342/NTU202303346

– i. turbulence and relaxation of idealized haloes. Mon Not Roy Astron Soc, 471(4):4559–4570, Jul 2017.

[9] Tomer D. Yavetz, Xinyu Li, and Lam Hui. Construction of wave dark matter halos: Numerical algorithm and analytical constraints. Phys. Rev. D, 105(2), jan 2022.

[10] Hsi-Yu Schive, John A ZuHone, Nathan J Goldbaum, Matthew J Turk, Massimo Gaspari, and Chin-Yu Cheng. gamer-2: a GPU-accelerated adaptive mesh refinement code – accuracy, performance, and scalability. Mon Not Roy Astron Soc, 481(4):4815–4840, sep 2018.

[11] Edward Seidel and Wai-Mo Suen. Dynamical evolution of boson stars: Perturbing the ground state. Phys. Rev. D, 42:384–403, Jul 1990.

[12] Lawrence M. Widrow and Nick Kaiser. Using the schroedinger equation to simulate collisionless matter. Astrophys J, 416:L71, Oct 1993.

[13] F. Siddhartha Guzman and L. Arturo Urena-Lopez. Gravitational cooling of self-gravitating bose condensates. Astrophys J, 645(2):814–819, Jul 2006.

[14] Hsi-Yu Schive, Tzihong Chiueh, and Tom Broadhurst. Cosmic structure as the quantum interference of a coherent dark wave. Nat Phys, 10(7):496–499, Jun 2014.

[15] Greg L. Bryan and Michael L. Norman. Statistical properties of x-ray clusters: Analytic and numerical comparisons. Astrophys J, 495(1):80–99, Mar 1998.

[16] Julio F. Navarro, Carlos S. Frenk, and Simon D. M. White. The structure of cold dark matter halos. Astrophys J, 462:563–575, May 1996.

[17] Nitsan Bar, Diego Blas, Kfir Blum, and Sergey Sibiryakov. Galactic rotation curves versus ultralight dark matter: Implications of the soliton-host halo relation. Phys. Rev. D, 98(8), Oct 2018.

[18] Atsushi Taruya and Shohei Saga. Analytical approach to the core-halo structure of fuzzy dark matter. Phys. Rev. D, 106(10), Nov 2022.

doi:10.6342/NTU202303346

[19] Andrés Bañares-Hernández, Andrés Castillo, Jorge Martin Camalich, and Giuliano Iorio. Confronting fuzzy dark matter with the rotation curves of nearby dwarf irregular galaxies, 2023.

[20] Fangzhou Jiang and Frank C. van den Bosch. Statistics of dark matter substructure –I. Model and universal fitting functions. Mon Not Roy Astron Soc, 458(3):2848–2869, Feb 2016.

[21] Angelo F. Neto, Liang Gao, Philip Bett, Shaun Cole, Julio F. Navarro, Carlos S. Frenk, Simon D. M. White, Volker Springel, and Adrian Jenkins. The statistics of Λ CDM halo concentrations. Mon Not Roy Astron Soc, 381(4):1450–1462, 10 2007.

[22] Hsi-Yu Schive, Tzihong Chiueh, and Tom Broadhurst. Soliton random walk and the cluster-stripping problem in ultralight dark matter. Phys Rev Lett, 124(20), may 2020.

doi:10.6342/NTU202303346